Microscopic Slip Boundary Conditions in Unsteady Fluid Flows

J. A. de la Torre,[1] D. Duque-Zumajo,[1] D. Camargo,[2] and Pep Español[1,*]
[1]Dept. Física Fundamental, Universidad Nacional de Educación a Distancia, Aptdo. 60141 E-28080, Madrid, Spain
[2]Facultad de Ingeniería y Arquitectura, Universidad Pontificia Bolivariana, CO-230003 Montería, Colombia

(Received 14 August 2019; published 24 December 2019)

An algebraic tail in the Green-Kubo integral for the solid-fluid friction coefficient hampers its use in the determination of the slip length. A simple theory for discrete nonlocal hydrodynamics near parallel solid walls with extended friction forces is given. We explain the origin of the algebraic tail and give a solution of the plateau problem in the Green-Kubo expressions. We derive the slip boundary condition with a microscopic expression for the slip length and the hydrodynamic wall position, and assess it through simulations of an unsteady plug flow.

DOI: 10.1103/PhysRevLett.123.264501

Hydrodynamics is a field theory described with partial differential equations that require the specification of boundary conditions for their solution. The no slip boundary condition has been successfully applied in the last two centuries in the solution of macroscopic flows [1]. However, as the length scale of observation is reduced towards the micro and nanoscale, a large number of experimental [2,3] and computer simulation studies [4–11] has shown that the fluid may actually slip along the container walls, a possibility first foreseen by Navier [12]. The fundamental understanding of the emergence of the slip boundary condition from microscopic principles may give useful information for the design of new microfluidics and nanofluidic devices ranging from water flow in confined carbon nanotubes (CNT) [13,14] and 2D atomic channels [15], flow in microarrays [16], and membrane filtration [17].

From the point of view of statistical mechanics, a boundary condition is just a way to take into account the effect of the solid walls on the fluid without having to explicitly describe the actual fluid-solid interactions. A seminal work by Bocquet and Barrat (BB) [18] showed that the slip coefficient is a transport coefficient given in terms of a Green-Kubo (GK) formula [19–25]. However, the BB GK formula for the friction coefficient does not display a plateau but decays algebraically, see Fig. 1. The definition of this transport coefficient is then ambiguous.

In this Letter, we provide a simple theory for the hydrodynamics of planar flows confined by planar solid walls. We can describe fluid-surface interactions in a rigorous way that allows in particular to properly define hydrodynamics at boundaries at nanoscales and gain intuition in these systems. We also compute from MD simulations the ensuing transport kernels, and validate the theory in nonequilibrium flow situations. The elements of the theory are the following. (i) The use of discrete hydrodynamic variables from the outset with a finite element methodology [26–29]. (ii) An intrinsic built-in length scale given by the discretization cell size that determines the level of coarse graining and allows us to discuss the role of non-Markovian effects. (iii) The effect of the solid walls appears explicitly as force terms within the hydrodynamic equations [30–32]. (iv) The hydrodynamic equations are nonlocal as has been advocated in the field of nanohydrodynamics [20,25,33–37]. (v) The GK expressions for the nonlocal kernels suffer from the plateau problem. We explain its hydrodynamic origin, and provide a solution [38]. (vi) The theory does not need boundary conditions, as the effect of the solid on the fluid is explicit, but allows us to derive them. (vii) A microscopic expression for the slip length and hydrodynamic wall position emerges. A more extensive account of these results is given in the accompanying paper [39].

Theory.—We consider a monoatomic fluid confined in between two parallel solid walls in the x, y directions. The normal axis z to the walls is divided in N_{bin} bins separated by nodal planes. We focus on the shear motion of the fluid and consider the parallel component $\hat{g}^x_\mu$ of the discrete momentum field defined on each nodal plane $\mu = 1, \ldots, N_{\mathrm{bin}}$.

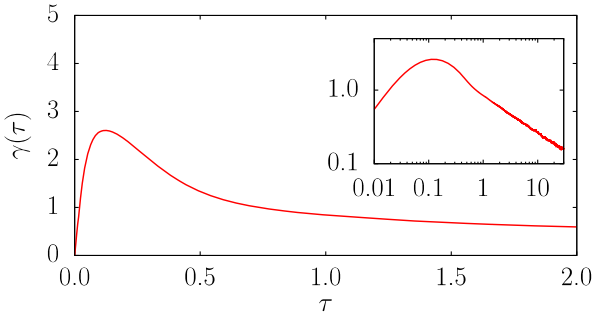

FIG. 1. The solid-liquid friction coefficient $\gamma(\tau)$ as a function of the upper limit of integration of the running GK integral defined in Eq. (10). Inset in log scale shows algebraic decay and absence of a plateau.

The microscopic definition of the discrete momentum is $\hat{\mathbf{g}}_\mu = \sum_i^N \mathbf{p}_i \delta_\mu(\mathbf{r}_i)$, where $\mathbf{r}_i$, $\mathbf{p}_i$ are the position and momentum of the ith atom and $\delta_\mu(\mathbf{r})$ is a one-dimensional finite element basis function corresponding to the μth nodal plane [32].

Mori theory [40–42] allows one to obtain exact closed equations for both the nonequilibrium average $g(t)$ of the discrete momentum density and the equilibrium time-correlation matrix $C(t) = \langle \hat{g}(t)\hat{g}^T \rangle$. The exact equations govern these quantities in terms of their past history through a memory kernel. Under a Markovian approximation, the exact integro-differential equations are approximated with simple linear ordinary differential equations—with no memory—of the form [38,39]

$$\frac{d}{dt} g(t) = -\Lambda^* g(t), \qquad \frac{d}{dt} C(t) = -\Lambda^* C(t), \tag{1}$$

where Λ^* is a relaxation matrix. Equations (1) describe exponential decay. Because of time reversibility $\dot{C}(0) = 0$, leading to the incorrect result $0 = -\Lambda^* C(0)$ at $t = 0$. Therefore, Eqs. (1) are valid only for times $t > \tau$, where τ is a time larger than the support of the memory kernel. Note that, according to Eq. (1) the matrix $\Lambda(t) \equiv -(d/dt)C(t)C^{-1}(t)$ should have a plateau given by Λ^* at and beyond the molecular time τ, this is $\Lambda(\tau) = \Lambda^*$. This will allow us to compute explicitly the relaxation matrix Λ^*.

An interesting form for the relaxation matrix is obtained from the following mathematical identity:

$$\frac{d}{dt} C(t) = -\int_0^t dt' \langle i\mathcal{L}\hat{g}(t') i\mathcal{L}\hat{g}^T \rangle = -k_B T M(t), \tag{2}$$

where $i\mathcal{L}$ is the Liouville operator and the matrix $M(t)$ is introduced here. As shown in Refs. [32,39], the momentum density changes as $i\mathcal{L}\hat{g}^x_\mu(z) = \hat{F}^x_\mu(z) - [(\hat{\sigma}^{xz}_\mu(z) - \hat{\sigma}^{xz}_{\mu-1}(z))/\Delta z]$, where $\hat{\mathbf{F}}_\mu$ is the force density that the solid exerts on the fluid on node μ and $\hat{\boldsymbol{\sigma}}_\mu$ is the local stress tensor of bin μ. In compact matrix form, this is $i\mathcal{L}\hat{g} = \hat{F} + \mathcal{D}^T\hat{\sigma}$, where the matrix $\mathcal{D}$ is the bi-diagonal forward finite difference operator. This leads in Eq. (2) to the decomposition

$$M(t) \equiv \mathcal{D}^T \eta(t) \mathcal{D} + G(t)\mathcal{D} + \mathcal{D}^T H(t) + \gamma(t), \tag{3}$$

where the $N_{\text{bin}} \times N_{\text{bin}}$ matrices $\eta(t)$, $G(t)$, $H(t)$, $\gamma(t)$ have as components the following GK running integrals

$$\eta_{\mu\nu} = \int_0^t dt' \frac{\langle \hat{\sigma}^{xz}_\mu(t')\hat{\sigma}^{xz}_\nu \rangle}{k_B T}, \quad G_{\mu\nu} = \int_0^t dt' \frac{\langle \hat{F}^x_\mu(t')\hat{\sigma}^{xz}_\nu \rangle}{k_B T},$$
$$H_{\mu\nu} = \int_0^t dt' \frac{\langle \hat{\sigma}^{xz}_\mu(t')\hat{F}^x_\nu \rangle}{k_B T}, \quad \gamma_{\mu\nu} = \int_0^t dt' \frac{\langle \hat{F}^x_\mu(t')\hat{F}^x_\nu \rangle}{k_B T}. \tag{4}$$

The matrix H is the transpose of the matrix G as a reflection of Onsager's reciprocity. Equations (2) and (3) relate correlations of momenta with correlations of stresses and forces. Equations (1), (2) allow us to express the relaxation matrix as

$$\Lambda^* = \Lambda(\tau) = k_B T M(\tau) C^{-1}(\tau), \tag{5}$$

so Eqs. (1) become

$$\frac{d}{dt} C(t) = -k_B T M(\tau) C^{-1}(\tau) C(t), \tag{6}$$

$$\frac{d}{dt} g(t) = -M(\tau)\mathcal{V}\bar{v}(t), \tag{7}$$

where we introduce the vector of scaled velocities as $\bar{v}(t) \equiv k_B T \mathcal{V}^{-1} C^{-1}(\tau) g(t)$, and the diagonal matrix $\mathcal{V}$ contains the volume elements of each bin. The scaled velocity is a momentum density divided by a mass density. Equations (6), (7) allow one to predict the dynamics from the knowledge of the computable GK expressions in Eqs. (3), (4). Note that $M(t)$ in Eq. (2), being proportional to $\dot{C}(t)$ decays to zero at long times, and so do the transport kernels (4). This is the plateau problem [41,43,44] that hinders the use of the GK formulas (4) to define transport kernels unambiguously. However, the present derivation of Eqs. (6), (7) for the discrete hydrodynamics allows us to use the plateau-problematic GK form (4) in such a way that the actual value of τ is irrelevant in the dynamics (6) and (7), provided that we are in the plateau region of $\Lambda(t)$ [38]. The exact results (2), (3) also explain why the GK nonlocal transport coefficients decay in a quasi-algebraic way, as this follows from the hydrodynamic decay of the momentum correlation matrix itself.

Finally, the discrete Eq. (7) with Eq. (3) can be understood as a finite element discretization of a nonlocal hydrodynamic continuum equation of the form [31]

$$\partial_t g(z,t) = \partial_z \int dz' \eta_{zz'} \partial_{z'} \bar{v}(z',t) - \partial_z \int dz' G_{zz'} \bar{v}(z',t)$$
$$- \int dz' H_{zz'} \partial_{z'} \bar{v}(z',t) - \int dz' \gamma_{zz'} \bar{v}(z',t). \tag{8}$$

The first term in the right-hand side in Eq. (8) involving second derivatives is a nonlocal viscosity term, while the other three terms reflect the irreversible force that the solid wall exerts on the fluid. The interaction with the walls is not described through boundary conditions but rather in terms of extended irreversible friction forces that appear directly in the hydrodynamic equations. This notion has been considered phenomenologically in Refs. [30,45] and theoretically in Refs. [31,32,46]. In Refs. [31,32,46] we disregarded the plateau problem present in the kernels $\eta_{zz'}, G_{zz'}, H_{zz'}, \gamma_{zz'}$, that is solved here by using the scaled velocity field $\bar{v}(z',t)$. While both the kernels and $\bar{v}$ depend on τ, the prediction of Eq. (8) for $g(t)$ is independent of τ.

Simulations.—We conduct MD simulations at equilibrium for a Lennard-Jones fluid (LJ) with parameters σ, ϵ in between two parallel walls [47–50]. A crude modeling of water with the LJ potential is obtained for $\sigma = 0.27$ nm and $\epsilon = 4.91 \times 10^{-21}$ J, $m = 30.1 \times 10^{-27}$ kg, and a time unit $\tau = \sigma(m/\epsilon)^{1/2} = 0.67$ ps [51]. The walls are made of simple cubic lattice crystals of fixed identical Lennard-Jones particles with lattice spacing $a = \sigma$ at a distance of 30σ corresponding to a channel width of ~ 8 nm. The thermodynamic point is given by a density in the bulk of $\rho = 0.6$ and a temperature $k_B T = 2.0$ in reduced units. Discrete momentum, forces, and stresses are measured, and their equilibrium correlations computed to obtain the correlation matrix $C(t)$ and the transport coefficients Eq. (4).

To confirm that the dynamics is given by the Markovian Eq. (1), we compute the eigenvalues $\tilde{\Lambda}_\mu(t) = -(d/dt)\tilde{C}_\mu(t)/\tilde{C}_\mu$ of $\Lambda(t)$, where $\tilde{C}_\mu(t)$ is the μth eigenvalue of the correlation matrix $C(t)$ [52]. Figure 2(a) shows that the eigenvalues $\tilde{\Lambda}_\mu(t)$ reach a clear plateau for the slowest modes. The bin size is $\Delta z = 0.5\sigma$, giving 60 bins and, therefore, 60 modes $\tilde{\Lambda}_\mu(t)$. At long times both $\tilde{C}_\mu(t)$ and its time derivative go to zero and its ratio is affected with large statistical errors. Therefore, we do not plot data for $\tilde{\Lambda}_\mu(t)$ when $\tilde{C}_\mu(t) < 10^{-5}$. Observe that the two fastest modes have identical eigenvalues $\tilde{C}_\mu(t)$ with a negative tail as shown in Fig. 2(b). A negative tail is incompatible with the exponential prediction of the Markov assumption. The eigenvectors of these modes are in the inset (c) in Fig. 2 and they describe near wall dynamics. Negative tails are observed for resolutions corresponding to bin sizes of $\Delta z = 0.5\sigma$ and $\Delta z = 1\sigma$. In contrast, for larger bins with $\Delta z = 2\sigma$ all modes decay exponentially [39] and the hydrodynamics at this coarser resolution is Markovian for times larger than τ. The physical origin of the non-Markovian behavior near

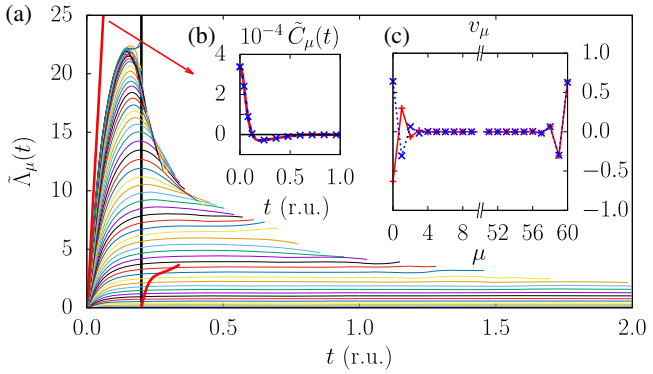

FIG. 2. (a) Eigenvalues $\tilde{\Lambda}_\mu(t)$ of the relaxation matrix $\Lambda(t)$, with faster modes in ascending order. One degenerate eigenvalue $\tilde{C}_\mu(t)$, signaled with an arrow and shown in the inset (b), becomes negative. The two eigenvectors v_μ of this eigenvalue in the inset (c) are highly localized near the walls. The vertical black line is at $\tau = 0.2$.

walls at high space resolution, with bin width smaller than the crystal lattice spacing, is probably due to a bounce-back caging effect of fluid molecules against the lattice crystal [53]. The results presented below are for a supramolecular bin size of $\Delta z = 2\sigma$ that behaves in a fully Markovian way for $t > \tau$. Better statistics for this bin width allow us to choose a slightly larger value for the plateau time $\tau = 0.3$ in reduced units.

The transport matrices $\eta(\tau)$, $G(\tau)$, $\gamma(\tau)$ are computed in terms of the GK running integrals (4). All of them decay in time, and in accord with the identity (2), showing no plateau. The nonlocal viscosity matrix η is concentrated along the diagonal and has a width of two bins, signaling stress correlations on a length scale of $\sim 4\sigma$. The matrices G, γ are localized near the nodes close to the walls and extend over distances of the order of two bins, 4σ, implying that irreversible wall effects are felt relatively far from the wall. With these transport matrices, we may now test the predictions (7) of the theory for an initial plug flow. This unsteady flow is challenging as it is initially discontinuous and gives large gradients near the walls. It is generated from an equilibrium atomic configuration by adding a constant velocity parallel to the walls to all fluid particles and rescaling to have the desired temperature. This nonequilibrium initial profile decays towards equilibrium at constant energy. The average over initial conditions of the momentum profile as a function of time is given in Fig. 3(a) where the initial plug flow evolves towards a decaying parabolic-like profile at large times, eventually settling to rest. The color code gives the error between the measured momentum and the prediction of the nonlocal theory (7). A zoom reveals disagreement at very short times smaller than the molecular time $\tau < 0.3$ when the early non-Markovian effects are appreciable even in the large bin case. However, the agreement of the nonlocal theory and simulation results is excellent beyond the molecular time τ.

Slip.—The slip boundary condition is obtained from the present theory as a mechanical balance. Consider a boundary slab of fluid made of B bins near one of the walls [20]. The total momentum of this slab is $P_B^x = \sum_{\mu=1}^{B} \mathcal{V}_\mu \hat{g}_\mu^x$. By using Eq. (7), the total force F_B^x on the slab is due to the combined action of the fluid outside the slab and the solid wall as [39]

$$\frac{1}{S}F_B^x = \sum_{\nu=1}^{B} \mathcal{V}_\nu \left((\eta_{B\nu} - G_\nu) \frac{\bar{v}_{\nu+1}^x - \bar{v}_\nu^x}{\Delta z} - (\gamma_\nu - H_{B\nu})\bar{v}_\nu^x \right). \quad (9)$$

The local transport coefficients are given by $G_\nu \equiv \sum_{\mu=1} \mathcal{V}_\mu G_{\mu\nu}/S$ and $\gamma_\nu \equiv \sum_{\mu=1} \mathcal{V}_\mu \gamma_{\mu\nu}/S$, where S is the surface area of the wall. Here, $\bar{v}_\nu^x$ are the components of the vector of scaled velocities $\bar{v}$ defined after Eq. (7). Assuming a parametric model for the fluid velocity profile, the mechanical balance (9) implies a condition on the parameters of the model. For a linear model, it implies a linear

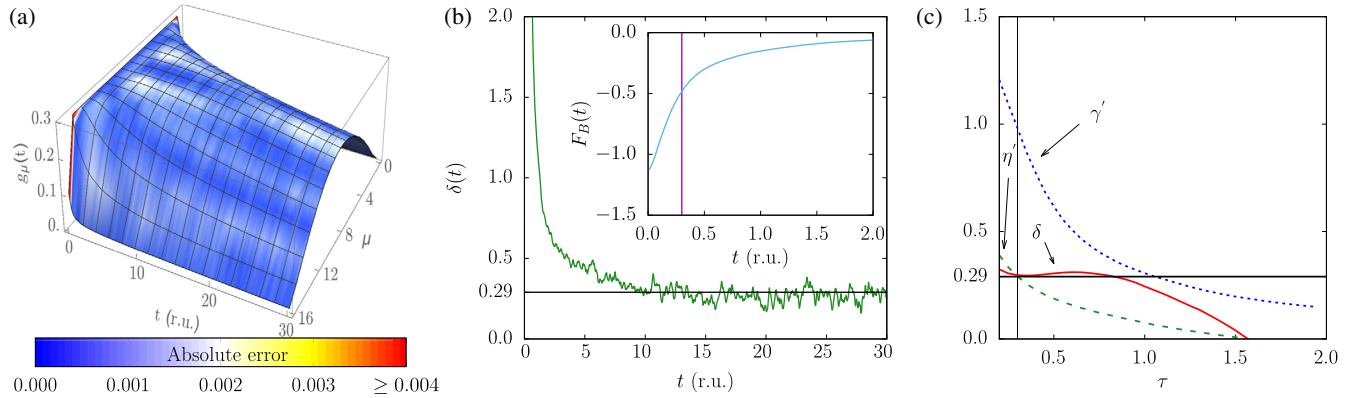

FIG. 3. (a) The measured discrete momentum $g_\mu(t)$ as a function of time for an initial plug flow. Color code denotes the absolute error of the nonlocal prediction (7). (b) The measured slip length $\delta(t)$ as a function of time. (c) The friction coefficient $\gamma' = \gamma - H$ (dotted blue), modified viscosity $\eta' = \eta - G$ (dashed green), and slip length δ (solid red), as a function of the upper limit of integration τ. The horizontal lines in (b), (c) show the predicted slip length $\delta = \eta'/\gamma' = 0.29$ in reduced units.

relationship between the velocity and the gradient at the wall position, leading to the slip boundary condition. Assume that the scaled velocity field in nodes $\mu = 1, \ldots, B$ inside the boundary slab is strictly linear and given by $\bar{v}^x_\mu = \bar{v}^x_{\rm wall} + \dot{\bar{\gamma}}_{\rm wall}(\mu\Delta z - z_{\rm wall})$, where $\bar{v}^x_{\rm wall}$ is the velocity at the wall position $z_{\rm wall}$, and $\dot{\bar{\gamma}}_{\rm wall}$ is the shear rate. Insertion of this linear velocity field in Eq. (9) leads to $(1/S)F^x_B = \eta'\dot{\bar{\gamma}}_{\rm wall} - \gamma'\bar{v}^x_{\rm wall}$, provided that the wall position is defined unambiguously from the friction properties of the wall as $z_{\rm wall} \equiv \{[\sum_\nu^B \mathcal{V}_\nu(\gamma_\nu - H_{B\nu})\nu\Delta z]/[\sum_\nu^B \mathcal{V}_\nu(\gamma_\nu - H_{B\nu})]\}$ [46]. The transport coefficients $\eta' = \eta - G$ and $\gamma' = \gamma - H$ are given as GK formulas

$$\eta = \int_0^\tau dt \frac{\langle \hat{\sigma}^{xz}_B(t)\hat{\sigma}^{xz}\rangle}{k_BT}, \qquad G = \int_0^\tau dt \frac{\langle \hat{F}^x(t)\hat{\sigma}^{xz}\rangle}{Sk_BT},$$
$$H = \int_0^\tau dt \frac{\langle \hat{\sigma}^{xz}_B(t)\hat{F}^x\rangle}{Sk_BT}, \qquad \gamma = \int_0^\tau dt \frac{\langle \hat{F}^x(t)\hat{F}^x\rangle}{Sk_BT}, \tag{10}$$

where $\hat{\mathbf{F}} = \sum_{ij'}^{NN'} \hat{\mathbf{F}}_{ij'}$ is the total force that the solid exerts on the fluid and $\hat{\boldsymbol{\sigma}} = \sum_i^N \mathbf{p}_i\mathbf{v}_i + \frac{1}{2}\sum_{ij}^N \mathbf{r}_{ij}\hat{\mathbf{F}}_{ij}$ is the total stress tensor of the fluid. These expressions emerge from summing over bins the nonlocal GK expressions (4). The values of η, G, H, γ, and $z_{\rm wall}$ depend on the width B of the boundary slab. We observe that beyond $B = 2$ these quantities become independent on B due to the finite range of the nonlocal transport kernels. Therefore, we select $B = 2$. For this width of the boundary slab we obtain $\eta = 0.84, G = 0.54, H = 0.01, \gamma = 1.00$ [r.u.]. The wall position $z_{\rm wall}$ is at a distance of 0.65σ from the crystal plane. The coefficient η coincides with the shear viscosity of the bulk fluid.

When $F^x_B(t) \simeq 0$ we obtain the Navier slip boundary condition $\bar{v}^x_{\rm wall} = \delta\dot{\bar{\gamma}}_{\rm wall}$ with the slip length given by the microscopic expression

$$\delta = \frac{\eta'}{\gamma'} = \frac{\eta - G}{\gamma - H}. \tag{11}$$

This prediction, involving not only stress and force autocorrelations through η, γ but also stress and force cross correlations through G, H is formally identical to the one that we have obtained in Ref. [46] from the continuum theory presented in Ref. [31]. As shown in Ref. [46], this microscopic expression for the slip length coincides with the one provided by BB [18] after a suitable redefinition of the wall position. The derivation of the microscopic expression of the slip length here gives, however, an additional information not evident in the continuum derivation presented in Ref. [46] or even in BB's derivation [18]. Note that the transport coefficients G, H, γ defined in Eq. (10) decay algebraically with τ, as seen in Fig. 1 for γ. Bocquet and Barrat [21] assumed that the thermodynamic limit would provide a cure for the plateau problem in the friction coefficient, but this is not correct. The solid-liquid friction coefficient γ does not display a plateau even in the thermodynamic limit [39]. Here, the plateau problem is solved by using the scaled velocity field $\bar{v}^x_\mu$, which depends on τ. Note that the slip boundary condition is predicated on the scaled velocity field. We observe in Fig. 3(c) that the slip length δ turns out to be rather insensitive to the actual value of τ, because this quantity is defined as a ratio of transport coefficients that decay with time in the same manner, at least around the time when the relaxation matrix reaches the plateau. A similar insensitivity is observed for the hydrodynamic wall position $z_{\rm wall}$.

To validate the prediction (11) against simulations we define the time-dependent slip length $\delta(t) = \bar{v}^x_{\rm wall}(t)/\dot{\bar{\gamma}}_{\rm wall}(t)$, where $\bar{v}^x_{\rm wall}(t)$ and $\dot{\bar{\gamma}}_{\rm wall}(t)$ are measured from a linear fit of the actual unsteady plug flow velocity profile near the wall. Figure 3(b) shows the measured $\delta(t)$ and the prediction (11). Only after a time $\simeq 5$ in reduced units the measured and predicted values coincide. This implies that the Navier slip

boundary condition is not satisfied for the plug flow in the very initial stages of the flow field shown in Fig. 3(a). This is because the force $F_B^x(t)$ on the boundary slab is nonzero at the early times $0.3 < t < 2$ [inset of Fig. 3(b)]. The curvature of the flow within the boundary slab explains the discrepancy for times $2 < t < 5$. After this time, good agreement with the prediction of the slip length is obtained.

Conclusions.—A simple theory for discrete nonlocal shear hydrodynamics near walls is proposed where the fluid-solid interaction is accounted for through friction forces that extend over a supramolecular distance $\sim 4\sigma$. The nonlocal transport kernels show algebraic tails and suffer from the plateau problem. In particular, the solid-fluid friction coefficient provided by BB is ill defined as it has no plateau. We use the method of Ref. [38] to solve the plateau problem in the GK transport kernels. The predictions of an unsteady plug flow with this nonlocal theory are very accurate. Also, we show that the slip boundary condition is not satisfied at the initial stages of an unsteady plug flow. The observation in this Letter that non-Markov effects in hydrodynamics are required when resolving flows at scales where density layering is important has far-reaching implications in the theoretical treatment of unsteady flows in confined geometries like CNT, as memory becomes an important ingredient in the theory. In addition, usual local descriptions based on the Navier-Stokes equations plus slip boundary conditions may not be entirely appropriate when the friction zones of the top and bottom walls overlap, which in our system is around a channel width of $L_z \sim 2$ nm.

Very useful discussions with Aleks Donev, Rafael Delgado-Buscalioni, Sophie Marbach, and Farid Chejne are highly appreciated. This research is supported by the Ministerio de Economía y Competitividad of Spain (MINECO) under Grant No. FIS2013-47350-C5-3-R and Ministerio de Ciencia, Innovación y Universidades under Grant No. FIS2017-86007-C3-3-P.

*pep@fisfun.uned.es

[1] G. Batchelor, *An Introduction to Fluid Dynamics* (Cambridge University Press, Cambridge, England, 1967).
[2] E. Lauga, M. P. Brenner, and H. A. Stone, in *Handbook Exp. Fluid Dynamics*, edited by C. Tropea, A. Yarin, and J. F. Foss (Springer, New York, 2007), pp. 1219–1240, Chap. 19.
[3] C. Cottin-Bizonne, A. Steinberger, B. Cross, O. Raccurt, and E. Charlaix, Langmuir **24**, 1165 (2008).
[4] P. A. Thompson and M. O. Robbins, Phys. Rev. A **41**, 6830 (1990).
[5] P. A. Thompson and S. M. Troian, Nature (London) **389**, 360 (1997).
[6] J. Koplik, Annu. Rev. Fluid Mech. **27**, 257 (1995).
[7] J.-l. Barrat and L. Bocquet, Phys. Rev. Lett. **82**, 4671 (1999).
[8] M. Cieplak, J. Koplik, and J. R. Banavar, Phys. Rev. Lett. **86**, 803 (2001).
[9] G. Karniadakis, A. Beskok, and N. Aluru, *Microflows and Nanoflows, Fundamentals and Simulation* (Springer Science+Business Media, Inc., New York, 2005).
[10] V. P. Sokhan and N. Quirke, Phys. Rev. E **78**, 015301 (2008).
[11] A. Sam, R. Hartkamp, S. K. Kannam, and S. P. Sathian, Nanotechnology **29**, 485404 (2018).
[12] M. Navier, Mem. Acad. R. Sci. Inst. France **6**, 389 (1827).
[13] S. K. Kannam, B. D. Todd, J. S. Hansen, and P. J. Daivis, J. Chem. Phys. **138**, 094701 (2013).
[14] J. Hassan, G. Diamantopoulos, D. Homouz, and G. Papavassiliou, Nanotechnol. Rev. **5**, 341 (2016).
[15] K. Gopinadhan, S. Hu, A. Esfandiar, F. C. Wang, Q. Yang, A. V. Tyurnina, A. Keerthi, B. Radha, and A. K. Geim, Science **363**, 145 (2019).
[16] M. K. Borg, D. A. Lockerby, K. Ritos, and J. M. Reese, J. Membr. Sci. **567**, 115 (2018).
[17] S. Balme, J.-M. Janot, L. Berardo, F. Henn, D. Bonhenry, S. Kraszewski, F. Picaud, and C. Ramseyer, Nano Lett. **11**, 712 (2011).
[18] L. Bocquet and J.-L. Barrat, Phys. Rev. E **49**, 3079 (1994).
[19] J. Petravic and P. Harrowell, J. Chem. Phys. **127**, 174706 (2007).
[20] J. S. Hansen, B. D. Todd, and P. J. Daivis, Phys. Rev. E **84**, 016313 (2011).
[21] L. Bocquet and J.-L. Barrat, J. Chem. Phys. **139**, 044704 (2013).
[22] K. Huang and I. Szlufarska, Phys. Rev. E **89**, 032119 (2014).
[23] S. Chen, H. Wang, T. Qian, and P. Sheng, Phys. Rev. E **92**, 043007 (2015).
[24] B. Ramos-Alvarado, S. Kumar, and G. P. Peterson, Phys. Rev. E **93**, 023101 (2016).
[25] P. J. Daivis and B. D. Todd, Processes **6**, 144 (2018).
[26] P. Español, J. G. Anero, and I. Zúñiga, J. Chem. Phys. **131**, 244117 (2009).
[27] P. Español and I. Zúñiga, J. Chem. Phys. **131**, 164106 (2009).
[28] J. A. de la Torre, P. Español, and A. Donev, J. Chem. Phys. **142**, 094115 (2015).
[29] P. Español and A. Donev, J. Chem. Phys. **143**, 234104 (2015).
[30] S. K. Bhatia and D. Nicholson, Langmuir **29**, 14519 (2013).
[31] D. Camargo, J. A. de la Torre, D. Duque-Zumajo, P. Español, R. Delgado-Buscalioni, and F. Chejne, J. Chem. Phys. **148**, 064107 (2018).
[32] D. Duque-Zumajo, D. Camargo, J. A. de la Torre, F. Chejne, and P. Español, Phys. Rev. E **99**, 052130 (2019).
[33] J. Zhang, B. D. Todd, and K. P. Travis, J. Chem. Phys. **121**, 10778 (2004).
[34] J. S. Hansen, P. J. Daivis, K. P. Travis, and B. D. Todd, Phys. Rev. E **76**, 041121 (2007).
[35] B. D. Todd, J. S. Hansen, and P. J. Daivis, Phys. Rev. Lett. **100**, 195901 (2008).
[36] B. A. Dalton, K. S. Glavatskiy, P. J. Daivis, B. D. Todd, I. K. Snook, B. A. Dalton, K. S. Glavatskiy, P. J. Daivis, and B. D. Todd, J. Chem. Phys. **139**, 044510 (2013).
[37] B. A. Dalton, K. S. Glavatskiy, P. J. Daivis, and B. D. Todd, Phys. Rev. E **92**, 012108 (2015).

[38] P. Español, J. A. de la Torre, and D. Duque-Zumajo, Phys. Rev. E **99**, 022126 (2019).
[39] D. Duque-Zumajo, J. de la Torre, D. Camargo, and P. Español, companion paper, Phys. Rev. E **100**, 062133 (2019).
[40] H. Mori, Prog. Theor. Phys. **33**, 423 (1965).
[41] R. Kubo, M. Toda, N. Hashitsume, and N. Saito, *Statistical Physics II: Nonequilibrium Statistical Mechanics* (Springer, Berlin, 1991).
[42] R. Zwanzig, *NonEquilibrium Statistical Mechanics* (Oxford University Press, Oxford, 2001).
[43] J. Kirkwood, F. Buff, and M. Green, J. Chem. Phys. **17**, 988 (1949).
[44] P. Español and I. Zúñiga, J. Chem. Phys. **98**, 574 (1993).
[45] V. P. Sokhan, D. Nicholson, and N. Quirke, J. Chem. Phys. **117**, 8531 (2002).
[46] D. Camargo, J. A. de la Torre, P. Español, R. Delgado-Buscalioni, and F. Chejne, J. Chem. Phys. **150**, 144104 (2019).
[47] S. Plimpton, J. Comput. Phys. **117**, 1 (1995).
[48] W. M. Brown, P. Wang, S. J. Plimpton, and A. N. Tharrington, Comput. Phys. Commun. **182**, 898 (2011).
[49] W. M. Brown, A. Kohlmeyer, S. J. Plimpton, and A. N. Tharrington, Comput. Phys. Commun. **183**, 449 (2012).
[50] W. M. Brown and Y. Masako, Comput. Phys. Commun. **184**, 2785 (2013).
[51] D. T. W. Lin and C. K. Chen, Acta Mech. **173**, 181 (2004).
[52] The eigenvectors of $C(t)$ do not change appreciably in time, as discussed in Ref. [39].
[53] For thermal walls made of moving atoms we expect that the bounce-back effect would be less pronounced and non-Markov effects less apparent.